Impurity Transport Caused by Blob and Hole Propagations

Hiroki Hasegawa[1,2] **and Seiji Ishiguro**[1,2]

[1] National Institute for Fusion Science (NIFS), National Institutes of Natural Sciences (NINS), Toki, Gifu, Japan

[2] Department of Fusion Science, SOKENDAI (The Graduate University for Advanced Studies), Toki, Gifu, Japan

E-mail: `hasegawa.hiroki@nifs.ac.jp`

December 2016

Abstract. It is for the first time demonstrated by means of the three-dimensional electrostatic Particle-in-Cell (PIC) simulation that the impurity ion transport caused by blob and hole propagations might not be negligible as compared with other types of transport. The simulations have shown that the impurity ion density profile in the blob / hole structure becomes a dipolar profile and the dipolar profile of the impurity ion density propagates with the blob / the hole. Furthermore, the simulations in which the initial impurity ion density has a radial gradient have revealed that the estimated effective radial diffusion coefficient for impurity ions by a single blob / hole is comparable to the Bohm diffusion coefficient.

PACS numbers: 52.55.-s, 52.25.Fi, 52.65.Rr, 52.27.Cm, 52.40.Hf

Keywords: blob, hole, scrape-off layer transport, impurity ion, particle-in-cell simulation
Submitted to: *Nucl. Fusion*

1. Introduction

The blob and the hole are the intermittent filamentary coherent structures along the magnetic field line in peripheral plasmas of fusion magnetic confinement devices, and the plasma densities in the blob and the hole are higher and lower than those of background plasma, respectively. These structures are thought to be created from edge turbulences, and they play an important role in the radial convective plasma transport in the scrape-off layer (SOL) [1, 2]. The blob phenomena have been observed in the tokamak, helical, and other devices [1, 3, 4, 5, 6, 7, 8, 9]. Although many authors have investigated the blob dynamics on the basis of two-dimensional reduced fluid models [1, 9], kinetic effects in the blob are reduced to adjustable parameters under some assumptions in such fluid

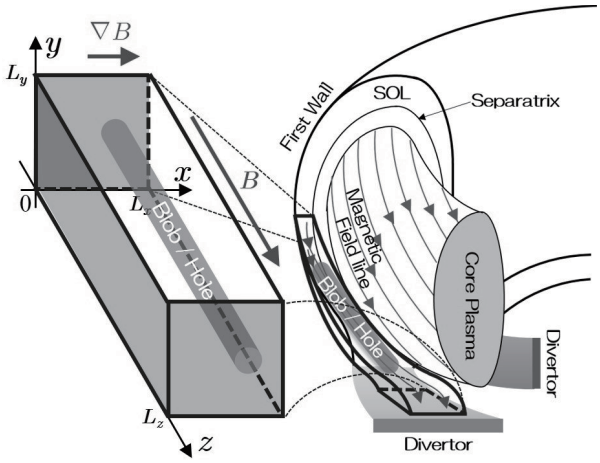

Figure 1. Schematic diagram of the simulation configuration. The slab box shown on the left side represents the simulation system which describes the SOL of magnetic confinement devices.

models. Thus, we have validated such assumptions with the first principles method, that is, the Particle-in-Cell (PIC) simulation, and confirmed that three-dimensional (3D) electrostatic PIC simulations provide an exact current closure for analysis of blob transports [10, 11, 12].

On the other hand, it has been pointed out that the blob and hole propagations can induce impurity ion transport [1, 13]. However, numerical studies regarding the impurity ion transport with the blob and the hole have not been conducted because of the difficulty in including minority ions, i.e., impurity ions, in fluid models. Therefore, in this study, we have developed the 3D-PIC code and investigated dynamics between impurity ions and the blob and hole structures. In Sec. 2, we briefly mention the simulation method, configuration, and parameters. In Sec. 3, we show particle simulation results and some properties of blob and hole propagations with impurity ions. Also, we estimate the impurity ion transports by a blob or by a hole in certain cases. Finally, we summarize our work in Sec. 4.

2. Simulation Methodology

In this study, we have investigated dynamics between impurity ions and the blob and hole structures by means of a three-dimensional electrostatic (the electric field is solved and the magnetic field is constant in time) PIC simulation code which calculates the full plasma particle (electron, ion, and impurity ion) dynamics (including the Larmor gyration motion) in three-dimensional space and three-dimensional velocity coordinates for all particles in a blob / hole structure and background plasma with the equation of motion. Also, the self-consistent electric field formed by the charge density that is calculated from all particles is solved with Poisson's equation in the code [14].

In the PIC simulation, an external magnetic field $\boldsymbol{B}$ is set as $\boldsymbol{B} = B(\boldsymbol{z}/z)$ and $\partial B/\partial x > 0$ (the $-x$, y, and z directions correspond to the radial, poloidal, and toroidal directions, respectively, as shown in Fig. 1). The external magnetic field strength B increases in the positive x direction as $B(x) = 2L_x B_{Lx}/(3L_x - x)$, where L_x, L_y, and L_z are the system size in the x, y, and z directions and B_{Lx} is the magnetic field strength at $x = L_x$. At $x = 0$ (corresponding to the first wall) and both edges in the z direction (corresponding to the divertor plates), the particle absorbing boundary where the electric potential ϕ is fixed as $\phi = 0$ is placed (i.e., shaded plates in Fig. 1). In the y direction, a periodic boundary condition is applied. At $x = L_x$, the reflecting boundary condition is adopted and the electric potential satisfies $\partial\phi/\partial x = 0$. A blob / a hole is initially set as a cylindrical form elongated between both edges in the z direction. That is, the electron and ion particles are initially distributed by

$$n_{\mathrm{e}0}(x, y) = n_0 \pm n_{\mathrm{b}0} \exp\left(-\frac{(x - x_{\mathrm{b}0})^2}{2\delta_{\mathrm{b}x}^2} - \frac{(y - y_{\mathrm{b}0})^2}{2\delta_{\mathrm{b}y}^2}\right), \tag{1}$$

and

$$n_{\mathrm{i}0}(x, y) = \frac{|q_{\mathrm{e}}|}{q_{\mathrm{i}}} n_{\mathrm{e}0}(x, y) - \frac{q_{\mathrm{imp}}}{q_{\mathrm{i}}} n_{\mathrm{imp}0}(x, y), \tag{2}$$

respectively. These initial electron and ion density equations include the blob / hole structure and background plasma. Here, n_0 is the initial density of the background plasma, $n_{\mathrm{b}0}$ is the initial density amplitude of the blob / the hole, $\delta_{\mathrm{b}x}$ and $\delta_{\mathrm{b}y}$ are the blob / hole sizes in the x and y directions, and q_{e}, q_{i}, and q_{imp} are the charges of electron, ion, and impurity ion. Equations (1) and (2) mean that the blob / the hole is initially located along the ambient magnetic field at around $(x, y) = (x_{\mathrm{b}0}, y_{\mathrm{b}0})$. The initial impurity ion density $n_{\mathrm{imp}0}$ is given by

$$n_{\mathrm{imp}0}(x, y) = n_{\mathrm{imp}1}, \tag{3}$$

(in the simulations shown in Sec. 3.1),

$$n_{\mathrm{imp}0}(x, y) = n_{\mathrm{imp}1} \exp\left(-\frac{(x - x_{\mathrm{b}0})^2}{2\delta_{\mathrm{b}x}^2} - \frac{(y - y_{\mathrm{b}0})^2}{2\delta_{\mathrm{b}y}^2}\right), \tag{4}$$

(in the simulations shown in Sec. 3.2), or

$$n_{\mathrm{imp}0}(x, y) = \frac{n_{\mathrm{imp}1}}{2}\left[1 - \tanh\left(\frac{x - x_{\mathrm{s}}}{\Delta_{\mathrm{s}}}\right)\right], \tag{5}$$

(in the simulations shown in Sec. 3.3) where $n_{\mathrm{imp}1}$ is the initial density amplitude of the impurity ion, x_{s} is the radial position of the boundary of the impurity ion region, and Δ_{s} is the width of the transition region. Equations (3)–(5) indicate that the impurity ions are distributed uniformly in the system, the impurity ions are placed in the blob / hole structure, and the impurity ions mainly exist on the first wall side ($x < x_{\mathrm{s}}$), respectively. The initial temperature in the blob is equal to that of the background plasma and the initial velocity distribution is given by Maxwellian. The simulation system has no particle and heat sources. Though the density distribution does not

satisfy equilibrium with the magnetic field, this assumption is appropriate in the low beta limit.

The simulation parameters are as follows. The number of spatial cells in the simulation system is set as $N_x \times N_y \times N_z = 64 \times 64 \times 256$ (in the simulations shown in Sec. 3.1) or $64 \times 64 \times 2048$ (in the simulations shown in Sec. 3.2 and Sec. 3.3), where $N_x = L_x/\Delta_{\rm g}$ and $\Delta_{\rm g}$ is the grid spacing whose size is approximately equal to 0.5 $\rho_{\rm s}$ in this study. Here, $\rho_{\rm s}$ is defined as $\rho_{\rm s} = c_{\rm s}/\Omega_{\rm i}$, $c_{\rm s}$ is the ion acoustic speed given as $c_{\rm s} = (T_{\rm e}/m_{\rm i})^{1/2}$, $\Omega_{\rm i}$ is the ion cyclotron frequency at $x = L_x$, $T_{\rm e}$ is the initial electron temperature, and $m_{\rm i}$ is the ion mass. The time step is $\Omega_{\rm i}\,\Delta t = 1.21 \times 10^{-3}$ (in the blob propagation simulations) or 1.26×10^{-3} (in the hole propagation simulations). The ion-to-electron and impurity-to-ion mass ratios are $m_{\rm i}/m_{\rm e} = 100$ and $m_{\rm imp}/m_{\rm i} = 4$ or 12. The charges are set as $-q_{\rm e} = q_{\rm i} = q_{\rm imp}$. The initial ion-to-electron and impurity-to-ion temperature ratios are $T_{\rm i}/T_{\rm e} = 0.01$ and $T_{\rm imp}/T_{\rm i} = 1$ (we assume low ion and impurity ion temperatures (i.e., small Larmor radiuses) in order to investigate fundamental dynamics). The external magnetic field strength is given as $\Omega_{\rm i}/\omega_{\rm pi} = 0.5$ where $\omega_{\rm pi}$ is the ion plasma frequency in the background plasma. The initial density ratio of the blob to the background plasmas is $n_{\rm b0}/n_0 = 2.7$ in the simulations of blob propagation. On the other hand, the initial density ratio between the center of the hole and the background is $(n_0 - n_{\rm b0})/n_0 = 0.27$ in the simulations of hole propagation. The initial blob / hole size is $\delta_{{\rm b}x} = \delta_{{\rm b}y} \approx 2\rho_{\rm s}$. The initial positions of the blob and the hole are $(x_{\rm b0}, y_{\rm b0}) = (3L_x/4, L_y/2)$ and $(L_x/2, L_y/2)$, respectively. The initial ratio between impurity ion and background electron densities is given as $n_{\rm imp1}/n_0 = 0.067$ (in the simulations of blob propagation) or 0.061 (in the simulations of hole propagation) since it is ~ 5 % in experiments for investigation of impurity transports (e.g., [15]). There are 72 electron simulation particles and about 68 ion simulation particles per cell on average. Also, there are about 70 impurity simulation particles per cell in the impurity region. (In PIC simulation, the simulation particle is "Superparticle" which contains a large number of real charged particles. The plasma parameters in PIC simulation do not depend on the number of real charged particles contained in a Superparticle because the charge-to-mass ratio is equal to that of the real particle [14]. In this study, the number of real impurity ions contained in the simulation particle of impurity ion is reduced than those of electron and ion in order to increase the number of simulation particles of impurity ion and improve the statistical property for impurity ion.) Although the electron and ion Larmor radiuses are smaller than the grid spacing in these parameters, the Larmor motion and the drift motions caused by gyration are resolved because the value of particle position has a real (continuous) number (not a discrete number). The charge density on the discrete grid points is calculated from the continuous particle position by the charge assignment and the force at the particles is calculated from the fields on the grid points by the interpolation in PIC simulation [14].

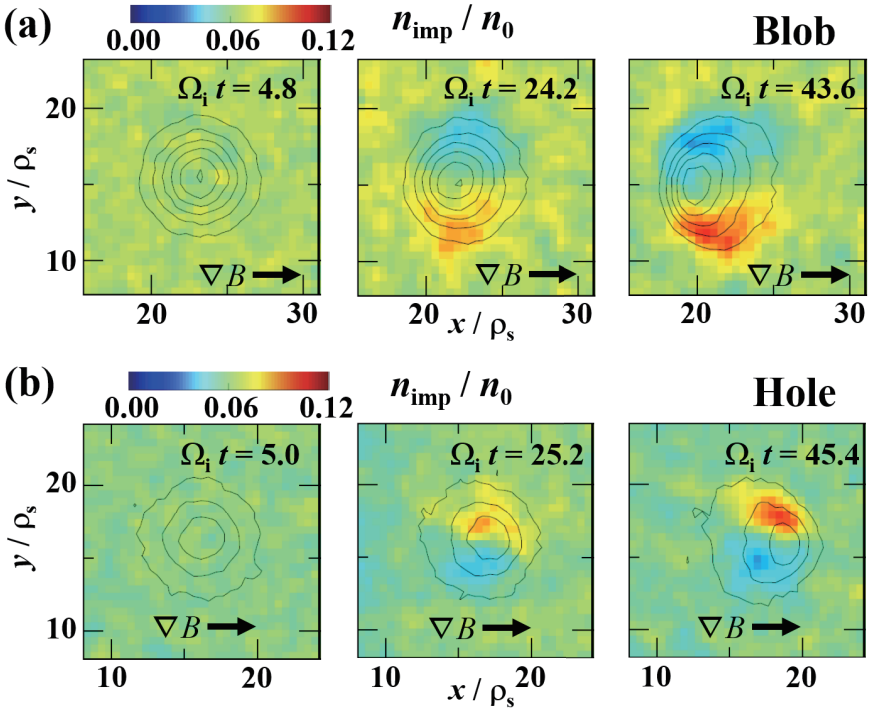

Figure 2. Impurity ion density distributions in poloidal cross-section at various times at $z = L_z/2$ with the blob (a) / hole (b) propagation, where the initial impurity ion density is spatially uniform and $m_{\rm imp}/m_{\rm i} = 4$. Here, the contour lines in each panel represent the electron density distributions.

3. Simulation Results

In this section, we introduce simulation results. In Sec. 3.1, we show simulation results of blob and hole propagations with uniformly distributed impurity ions. In Sec. 3.2, the dynamics of impurity ions which are initially placed in a blob / hole structure are shown. In Sec. 3.3, we present simulation results of impurity ion transport from the first wall side in the grad-B direction by blob / hole propagation and estimate an effective diffusion coefficient.

3.1. Blob / Hole Propagation with Uniformly Distributed Impurity Ions

Figure 2 shows results of simulations in which the initial impurity ion density is spatially uniform as Eq. (3). As seen from Figs. 2 (a) and (b), it is shown that impurity ions in the blob / the hole are dragged from the higher to the lower potential sides (the dipole potential structure on the poloidal cross-section is created in a blob / a hole [11, 12]) by the polarization drift and that the dipolar profile of impurity ion density is transported with the blob / the hole by trapping impurity ions in the potential well of the blob / the hole. Figure 3 indicates that the propagation speed of the blob / the hole with impurity ions is nearly equal to that without impurity ions. On the other hand, the fact that

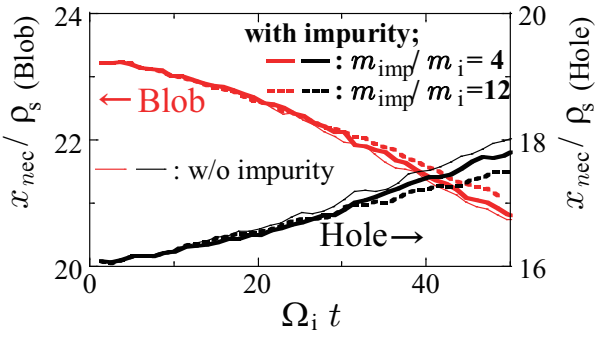

Figure 3. Evolution of the x position of the electron center of mass of the blob (red lines) / the hole (black lines) at $z = L_z/2$ with impurity ions (thick solid and broken lines) / without impurity ions (thin lines).

the propagation speed becomes slightly slower as the impurity ion mass increases proves that the dipolar profile of impurity ion density arises from the polarization drift.

In order to prove the mechanism mentioned above quantitatively, we consider the theoretical estimation of impurity ion density with the continuity equation by the method similar to the analysis shown in [16] in which impurity clusters in vortices were observed in edge turbulence by the numerical simulation based on the two-dimensional Hasegawa-Wakatani model with the impurity passive-fluid model. The continuity equation is given as

$$\frac{\mathrm{D}\, n_{\mathrm{imp}}}{\mathrm{D}\, t} + n_{\mathrm{imp}} \boldsymbol{\nabla} \cdot (\boldsymbol{v}_{\mathrm{E}} + \boldsymbol{v}_{\mathrm{g}} + \boldsymbol{v}_{\mathrm{p}}) = 0, \tag{6}$$

where $\mathrm{D}/\mathrm{D}t$ represents $\partial/\partial t + \boldsymbol{v}_{\mathrm{imp}} \cdot \boldsymbol{\nabla}$ (the Lagrangian derivative), $\boldsymbol{v}_{\mathrm{imp}}$ is defined as $\boldsymbol{v}_{\mathrm{imp}} = \boldsymbol{v}_{\mathrm{E}} + \boldsymbol{v}_{\mathrm{g}} + \boldsymbol{v}_{\mathrm{p}}$, and $\boldsymbol{v}_{\mathrm{E}}$, $\boldsymbol{v}_{\mathrm{g}}$, and $\boldsymbol{v}_{\mathrm{p}}$ are the $E \times B$, the grad-B, and the polarization drift velocities, respectively. Since the magnetic field is parallel to the z axis, the compression by the grad-B drift is zero, the compression by the $E \times B$ drift is negligible, and the polarization drift velocity is given as

$$\boldsymbol{v}_{\mathrm{p}} = -\frac{m_{\mathrm{imp}}}{q_{\mathrm{imp}} B^2} \frac{\mathrm{D}\, (\boldsymbol{\nabla}\phi)}{\mathrm{D}\, t}, \tag{7}$$

Eq. (6) becomes

$$\frac{\mathrm{D}}{\mathrm{D}\, t} \left[\ln\left(n_{\mathrm{imp}}\right) - \zeta \Phi \right] \approx 0. \tag{8}$$

Thus, we obtain the theoretical estimation of impurity ion density as

$$n_{\mathrm{imp}} \approx n_{\mathrm{imp0}} \exp(\zeta \Phi), \tag{9}$$

where Φ and ζ are defined as

$$\Phi = \frac{m_{\mathrm{i}}}{q_{\mathrm{i}} B^2} \left(\boldsymbol{\nabla}^2 \phi - \frac{2}{B} \frac{\partial B}{\partial x} \frac{\partial \phi}{\partial x} \right), \tag{10}$$

and

$$\zeta = \frac{m_{\mathrm{imp}}/q_{\mathrm{imp}}}{m_{\mathrm{i}}/q_{\mathrm{i}}}, \tag{11}$$

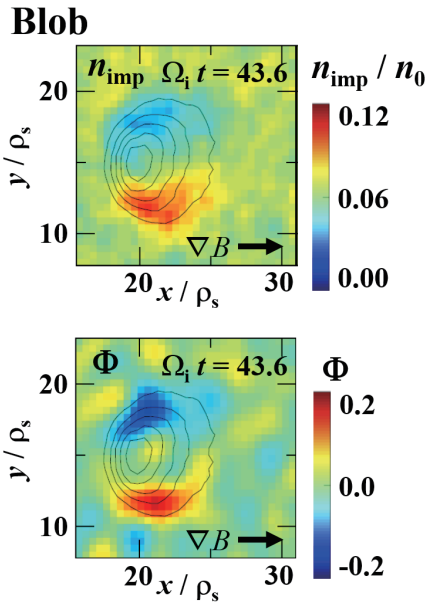

Figure 4. Impurity ion density (top panel) and Φ (bottom panel) distributions in poloidal cross-section at $\Omega_i t = 43.6$ at $z = L_z/2$ with the blob propagation. Here, the contour lines in each panel represent the electron density distributions.

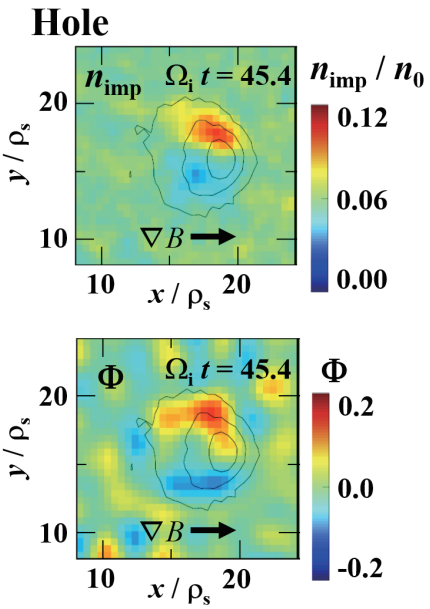

Figure 5. Impurity ion density (top panel) and Φ (bottom panel) distributions in poloidal cross-section at $\Omega_i t = 45.4$ at $z = L_z/2$ with the hole propagation. Here, the contour lines in each panel represent the electron density distributions.

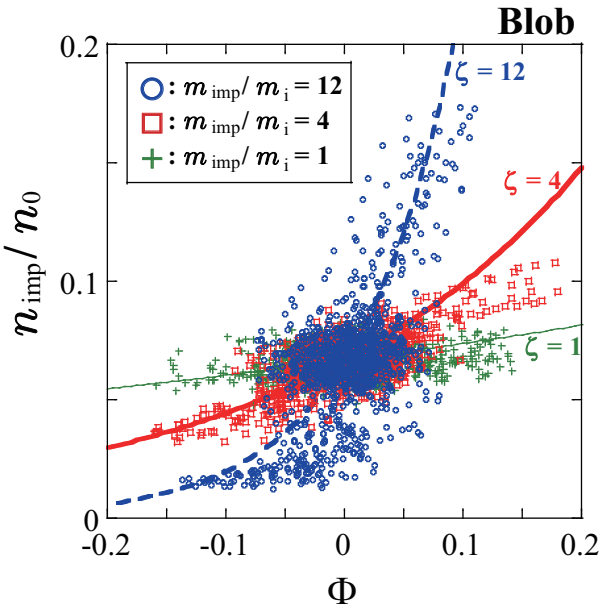

Figure 6. Scatter plot of Φ and impurity ion density at $\Omega_i t = 43.6$ with the blob propagation. The blue open circles, the red square, and the green pluses represent the results in the cases where $m_{imp}/m_i = 12$, 4, and 1, respectively. Also, the blue broken, the red thick solid, and the green thin solid lines present the theoretical estimations given by Eq. (9) when $\zeta = 12$, 4, and 1. The dots plotted in the panel show the values of Φ and n_{imp} on the grid points in the region shown in Fig. 4.

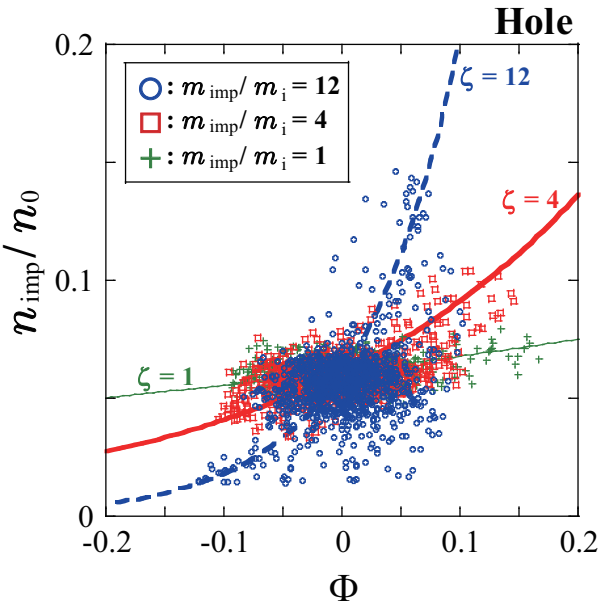

Figure 7. Scatter plot of Φ and impurity ion density at $\Omega_i t = 45.4$ with the hole propagation. The blue open circles, the red square, and the green pluses represent the results in the cases where $m_{imp}/m_i = 12$, 4, and 1, respectively. Also, the blue broken, the red thick solid, and the green thin solid lines present the theoretical estimations given by Eq. (9) when $\zeta = 12$, 4, and 1. The dots plotted in the panel show the values of Φ and n_{imp} on the grid points in the region shown in Fig. 5.

respectively. The variable Φ corresponds to the vorticity of the $E \times B$ drift velocity in the two-dimensional analysis. Figures 4 and 5 indicate the correlation between the distribution of impurity ion density and that of Φ as expected by Eq. (9). Furthermore, the scatter plots of Φ and impurity ion density seen in Figs. 6 and 7 show that the observed impurity ion density is in agreement with the theoretical estimation. This fact means that the dipolar profile of impurity ion density occurs by the compressibility introduced by the polarization drift. The similar correlation between the vorticity and the impurity ion density was observed in the two-dimensional fluid simulation of plasma turbulence [16]. Though the impurity ion has not made one cyclotron motion completely in the case where $m_{\rm imp}/m_{\rm i} = 12$ in Figs. 6 and 7, it is thought that the averaged impurity ion velocity has become comparable to the polarization drift velocity with the acceleration by the electric field, that is, the drift approximation in the above discussion may be available. On the other hand, if the charge (i.e., ionization degree) of an impurity ion is changed by collisions during the propagation of a blob / a hole, the variation of impurity ion charge could influence the impurity ion density distribution because the modulation of impurity ion density depends on ζ, i.e., the charge-to-mass ratio as shown in Eq. (9).

Although the blob / hole propagation is hardly influenced by the impurity ions, the impurity ions in the blob / the hole move in the $\mp\nabla B$ direction as shown in Fig. 8. The impurity ion averaged radial speed in the blob / the hole is close to the blob / hole propagation speed obtained as $v_{\rm b} = -0.064\, c_{\rm s}$ or $v_{\rm h} = 0.045\, c_{\rm s}$ from Fig. 3.

3.2. Dynamics of Impurity Ion in a Blob / Hole Structure

Figure 9 presents results of simulations in which impurity ions are initially placed in a blob / hole structure as Eq. (4). Although the previous simulations seen in Sec. 3.1 do not demonstrate actual impurity ion transport clearly, Fig. 9 indicates that most of the impurity ion particles which stay in the blob / hole structure at the initial stage are transported with the blob / the hole after shaping the dipolar profile through the polarization drift. Figures 10 and 11 show the time evolutions of the positions of the impurity ion center of mass with the blob and hole propagations, respectively. In Figs. 10 and 11 it is found that the impurity ion center of mass moves with the blob and the hole. Also, the evolution of the y position of the impurity ion center of mass in the hole propagation case shown in Fig. 11 proves that many impurity ions are dragged to the lower potential side by the polarization drift. However, the impurity ion center of mass does not tend to go to the lower potential side in the blob propagation case seen in Fig. 10. This fact is thought to arise from the thin spread of impurity ions around the potential well as shown in the center and right panels of Fig. 9 (a).

3.3. Impurity Transport by Blob / Hole Propagation

Figures 12 and 13 show results of simulations in which the initial impurity ion density has a radial gradient as Eq. (5). Here, the radial position of the boundary of the

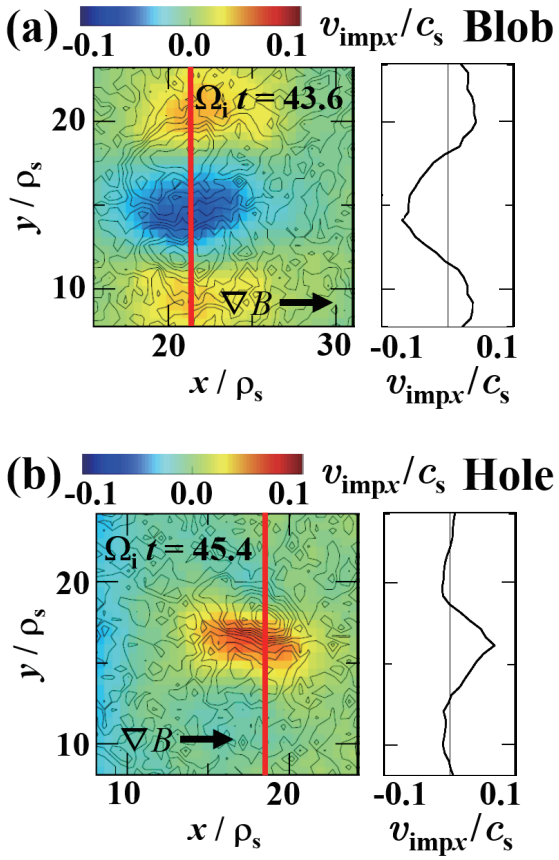

Figure 8. Distributions of the x components of impurity ion averaged velocity in the blob (a) and hole (b) cases at $z = L_z/2$, where $m_{\rm imp}/m_{\rm i} = 4$. In each figure, the left panel shows the 2D profile in the poloidal plane, while the right panel presents the 1D profile along the red line at $x = 21.3\rho_{\rm s}$ (a) or $18.7\rho_{\rm s}$ (b) in the 2D profile. Here, the contour lines in the 2D profiles represent the impurity ion density.

impurity ion region and the width of the transition region are set as $x_{\rm s} = 5L_x/8$ and $\Delta_{\rm s} = 8\Delta_{\rm g} \approx 4\rho_{\rm s}$. In the case of blob propagation shown in Fig. 12, the blob is initially located in a region without impurity ions ($x > x_{\rm s}$) since $x_{\rm b0} = 3L_x/4$ and $x_{\rm s} = 5L_x/8$. Then, the blob penetrates to the impurity ion region ($x < x_{\rm s}$). Figure 12 indicates that the blob sweeps impurity ions with the blob propagation and that the impurity ions which surround the blob move in the grad-B direction by the $E \times B$ drift.

On the other hand, in the case of hole propagation shown in Fig. 13, the hole is initially placed in the impurity region ($x < x_{\rm s}$) since $x_{\rm b0} = L_x/2$ and $x_{\rm s} = 5L_x/8$. Then, the hole moves from the impurity region gradually. Figure 13 demonstrates that the hole carries impurity ions in the grad-B direction.

Although the blob, the hole, and the impurity ion transport by the blob and hole propagations are convective, we have considered the effective radial diffusion coefficients for impurity ions by the blob and hole propagations in order to compare that transport with conventional diffusive transports. The effective radial diffusion coefficient $D_{\rm imp\perp}$

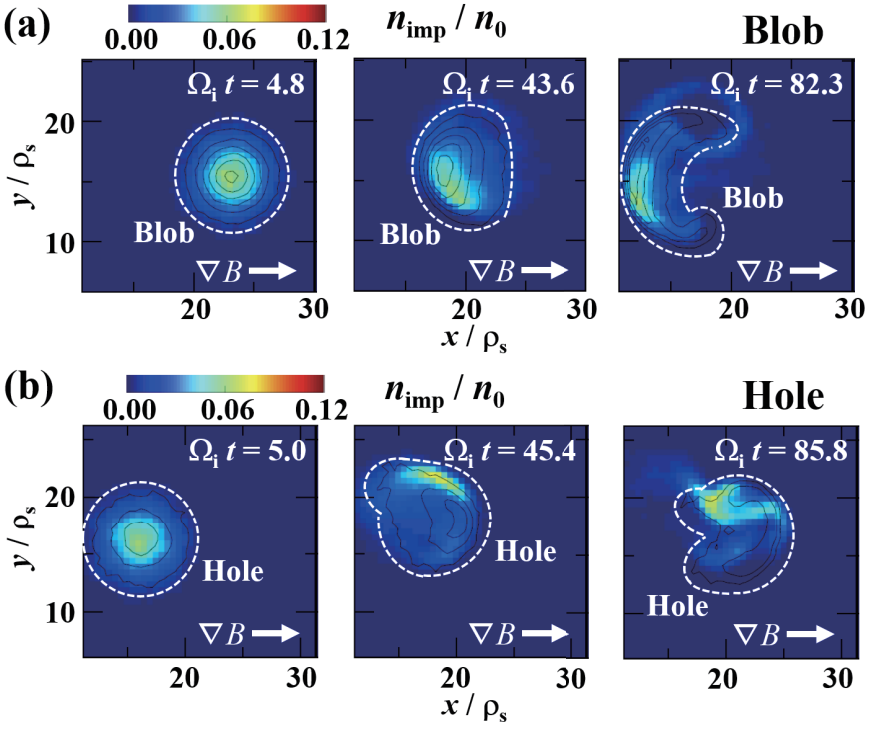

Figure 9. Impurity ion density distributions in poloidal cross-section at various times at $z = L_z/2$ with the blob (a) / hole (b) propagation, where impurity ions are initially located in the blob / the hole and $m_{imp}/m_i = 4$. Here, the contour lines in each panel represent the electron density distributions.

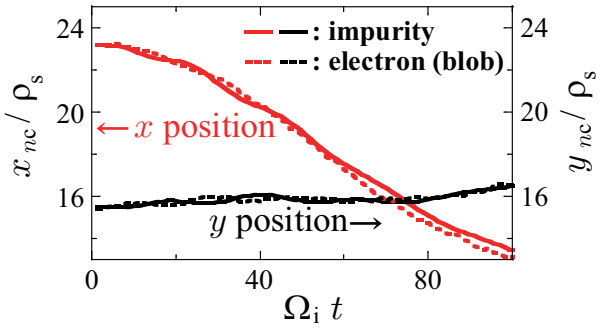

Figure 10. Evolutions of the x (red lines) and y (black lines) positions of the impurity ion center of mass at $z = L_z/2$ with the blob propagation. The solid and broken lines represent the spatial variations of the impurity ion center of mass and the electron (in the blob) center of mass, respectively.

is calculated from the impurity ion radial flux $\Gamma_{imp\perp}$ on y-z plane at $x = x_s$ in the simulation system by

$$D_{imp\perp} = \frac{\Gamma_{imp\perp}}{\nabla_\perp n_{imp}} \approx \frac{2\,\Delta_s\,\Gamma_{imp\perp}}{n_{imp1}}. \tag{12}$$

The effective radial diffusion coefficients in the simulations seen in Figs. 12 and 13 are

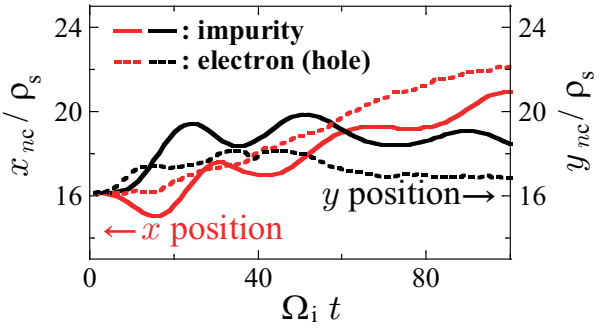

Figure 11. Evolutions of the x (red lines) and y (black lines) positions of the impurity ion center of mass at $z = L_z/2$ with the hole propagation. The solid and broken lines represent the spatial variations of the impurity ion center of mass and the electron (in the hole) center of mass, respectively.

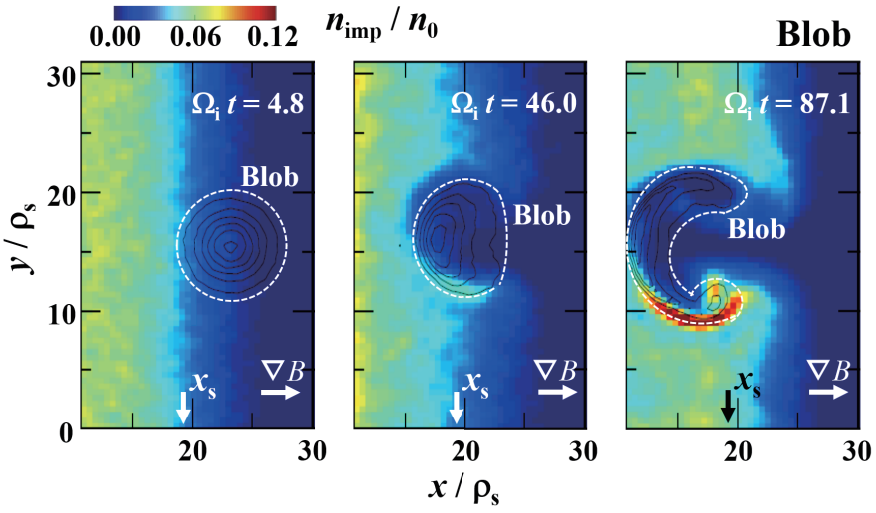

Figure 12. Impurity ion density distributions in poloidal cross-section at various times at $z = L_z/2$ with the blob propagation, where the initial impurity ion density has a radial gradient, $x_s = 19.4\,\rho_s$, and $m_{imp}/m_i = 4$. Here, the contour lines in each panel represent the electron density distributions.

obtained as $D_{imp\perp}/D_B = 2.66$ and 1.26, respectively, where D_B is the Bohm diffusion coefficient defined as $D_B = T_e/(16|q_e|B_{Lx})$. Here, $\Gamma_{imp\perp}$ is provided with the averaged flux between $\Omega_i\, t = 1.2$ and 116.2 (the blob case) / $\Omega_i\, t = 1.3$ and 117.3 (the hole case). Although the coefficient by the blob is larger than that by the hole, it is obvious that the hole transports impurity ions further from the impurity region than does the blob.

4. Summary and Discussion

This study first shows the following facts regarding dynamics between impurity ions and the blob / hole structure by means of the 3D-PIC simulation: (1) the dipolar profile of

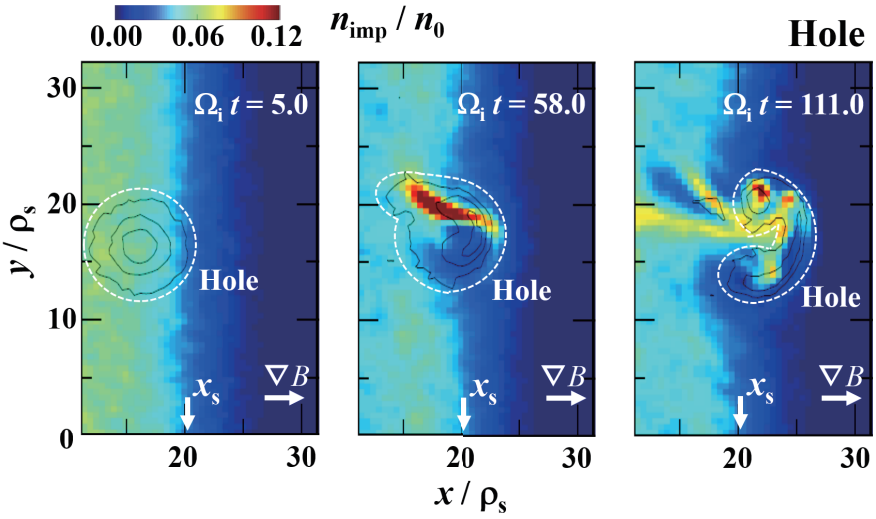

Figure 13. Impurity ion density distributions in poloidal cross-section at various times at $z = L_z/2$ with the hole propagation, where the initial impurity ion density has a radial gradient, $x_s = 20.2\,\rho_s$, and $m_{imp}/m_i = 4$. Here, the contour lines in each panel represent the electron density distributions.

impurity ion density in the blob / the hole is formed, (2) such a density profile propagates with the blob / the hole, and (3) the effective radial diffusion coefficient for impurity ions by a single blob / hole is comparable to the Bohm diffusion coefficient. Although, of course, the effective diffusion coefficient should be multiplied by the production rate of blobs / holes per time and area to calculate an actual coefficient, such a type of transport might not be negligible as compared with other types of transport because it was observed that the ratio between the radial particle flux by the blob and the total radial particle flux is ~ 0.5 in the tokamak experiment [3]. Furthermore, the impurity ion transport by the blob / the hole might be able to explain the difference of impurity transport property between tokamak and helical devices since the blob / hole propagation direction in helical devices is opposite to that in the tokamak devices (low-field side).

Acknowledgments

The authors are grateful to Prof. S. I. Krasheninnikov (UCSD) and Prof. A. Hatayama (Keio Univ.) for stimulating discussions. The simulations were carried out on the Plasma Simulator (PS) of the National Institute for Fusion Science (NIFS) and the high-performance computer system of Nagoya University. This work is performed with the support and under the auspices of the NIFS Collaboration Research programs (NIFS15KNSS058, NIFS14KNXN279, NIFS15KNTS039, NIFS15KNTS040, and NIFS16KNTT038), supported by a Grant-in-Aid for Scientific Research from the Japan Society for the Promotion of Science (KAKENHI 23740411), and

partially supported by "Joint Usage/Research Center for Interdisciplinary Large-scale Information Infrastructures" and "High Performance Computing Infrastructure" in Japan.

References

[1] Krasheninnikov S. I. *et al* 2008 *J. Plasma Phys.* **74** 679 and references therein
[2] Krasheninnikov S. I. 2001 *Phys. Lett.* A **283** 368
[3] Boedo J. A. *et al* 2001 *Phys. Plasmas* **8** 4826
[4] Antar G. Y. *et al* 2003 *Phys. Plasmas* **10** 419
[5] Maqueda R. J. *et al* 2001 *Rev. Sci. Instrum.* **72** 931
[6] Boedo J. A. *et al* 2003 *Phys. Plasmas* **10** 1670
[7] Tanaka H. *et al* 2010 *Phys. Plasmas* **17** 102509
[8] de la Cal E. *et al* 2014 *Plasma Phys. Control. Fusion* **56** 105003
[9] D'Ippolito D. A. *et al* 2011 *Phys. Plasmas* **18** 060501 and references therein
[10] Ishiguro S. and Hasegawa H. 2006 *J. Plasma Phys.* **72** 1233
[11] Hasegawa H. and Ishiguro S. 2012 *Plasma Fusion Res.* **7** 2401060
[12] Hasegawa H. and Ishiguro S. 2015 *Phys. Plasmas* **22** 102113
[13] Krasheninnikov S. I. *et al* 2003 *Proc. 19th IAEA Fusion Energy Conf. (Lyon, France, 2002)* (Vienna: International Atomic Energy Agency) IAEA-CN-94/TH/4-1
[14] Birdsall C. K. and Langdon A. B. 1985 *Plasma Physics via Computer Simulation* (New York: McGraw-Hill Book Company)
[15] Yoshinuma M. *et al* 2009 *Nucl. Fusion* **49** 062002
[16] Priego M. *et al* 2005 *Phys. Plasmas* **12** 062312